RESEARCH ARTICLE SUMMARY

BLOOD STEM CELLS

Regulation of the hematopoietic stem cell pool by C-Kit–associated trogocytosis

Xin Gao*†, Randall S. Carpenter†, Philip E. Boulais†, Dachuan Zhang, Christopher R. Marlein, Huihui Li, Matthew Smith, David J. Chung, Maria Maryanovich, Britta Will*†, Ulrich Steidl*†, Paul S. Frenette†

INTRODUCTION: Hematopoietic stem cells (HSCs) produce all types of blood cells and ensure lifelong maintenance and replenishment of the hematopoietic system. These adult stem cells reside in a specialized microenvironment in the bone marrow (BM) yet show a distinctive behavior whereby a small fraction of their population continuously egresses from the BM to travel into blood circulation—a process termed "stem cell mobilization." This property is harnessed in the clinic by enforcing HSC mobilization through pharmacological modulation of hematopoietic cytokine signaling through exposure to granulocyte colony-stimulating factor (G-CSF) or C-X-C chemokine receptor type 4 (CXCR4) antagonists. Mobilized HSCs are harvested from the peripheral blood for subsequent hematopoietic stem cell transplantation, e.g., for treatment of patients with cancer, autoimmune, and other disorders.

RATIONALE: The mechanisms governing mobilization of individual HSCs into the blood are incompletely understood. Moreover, current therapeutic regimens fall short in stimulating BM egress of sufficient numbers of HSCs in a sizable proportion of patients. We there analyzed the proteins expressed on the su of HSCs isolated from mice and investigated the mechanisms underlying the ability of most HSCs to be retained in BM while others can be mobilized.

RESULTS: We found that a large subset of HSCs displayed macrophage-associated markers, including F4/80 and CD169, on their cell surface. We assessed long-term regenerative multilineage repopulation capacity and the ability to mobilize from the BM upon forced mobilization or aging in HSCs expressing or not expressing macrophage markers. Macrophage marker–presenting HSCs were fully functional and largely retained in the BM, whereas stem cells without detectable macrophage-marker presentation readily exited the BM upon forced mobilization. Using in vitro cocultures of HSCs and macrophages, we discovered that HSCs could use trogocytosis ($TROG^{Pos}$ HSCs)—a rapid and active transfer mechanism for surface molecules in which plasma membrane fragments are trafficked from one cell to another. Trogocytosis was impaired in the presence of stem cell factor. We therefore utilized genetic and pharmacological mouse models, as well as primary human cell–based assays, to trace how macrophage membrane material could be transferred onto HSCs. These efforts identified receptor tyrosine kinase C-Kit as a marker of stem cell trogocytosis and showed that HSCs with high C-Kit presentation on their cell surface could engage this mechanism to acquire CXCR4 from adjacent macrophages to increase stem cell retention in the niche.

CONCLUSION: We uncovered a definable pool of mobilizable stem cells and demonstrated that membrane-fragment transfer from macrophages could be functionalized by HSCs for BM retention. Our study provides proof of concept that adult stem cells can utilize trogocytosis to establish and activate function-modulating molecular mechanisms rapidly. These findings have implications for the development of more effective HSC mobilization strategies in the clinic, potentially through exploiting pharmacologic impairment of C-Kit. They will also spark efforts into delineating how much HSCs use trogocytosis to acutely gain function in other contexts, as well as the extent to which the hematopoietic system may use trogocytosis-mediated cell killing for eliminating defective stem cells. ■

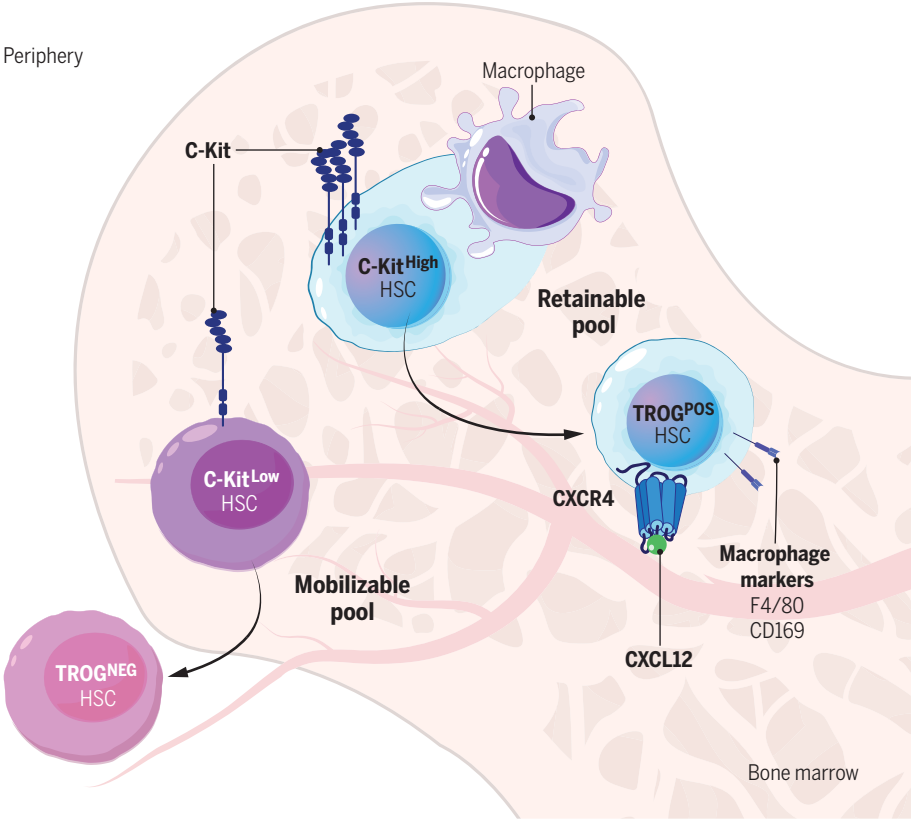

ILLUSTRATION: TATYANA A. HARRIS FROM THE EINSTEIN CREATIVE SERVICES TEAM

Model for C-Kit–dependent trogocytosis regulates niche retention in blood stem cells. A subset of HSCs (marked by high C-Kit expression) can acquire membrane material from adjacent macrophages through trogocytosis ($TROG^{Pos}$ HSC) to augment retention in the bone marrow. Stem cells with low C-Kit expression are mobilized to the peripheral blood.

The list of author affiliations is available in the full article online.
*Corresponding author. Email: xgao37@wisc.edu (X.G.); britta.will@einsteinmed.edu (B.W.); ulrich.steidl@einsteinmed.edu (U.S.)
†These authors contributed equally to this work.
Cite this article as X. Gao *et al.*, *Science* **385**, eadp2065 (2024). DOI: 10.1126/science.adp2065

READ THE FULL ARTICLE AT
https://doi.org/10.1126/science.adp2065

RESEARCH ARTICLE

BLOOD STEM CELLS

Regulation of the hematopoietic stem cell pool by C-Kit–associated trogocytosis

Xin Gao[1,2,3]*†, Randall S. Carpenter[1,2]†, Philip E. Boulais[1,2]†‡, Dachuan Zhang[1,2,4], Christopher R. Marlein[1,2], Huihui Li[1,2], Matthew Smith[3], David J. Chung[5], Maria Maryanovich[1,2,6], Britta Will[1,2,6,7,8]*†, Ulrich Steidl[1,2,6,7]*†, Paul S. Frenette[1,2]†§

Hematopoietic stem cells (HSCs) are routinely mobilized from the bone marrow (BM) to the blood circulation for clinical transplantation. However, the precise mechanisms by which individual stem cells exit the marrow are not understood. This study identified cell-extrinsic and molecular determinants of a mobilizable pool of blood-forming stem cells. We found that a subset of HSCs displays macrophage-associated markers on their cell surface. Although fully functional, these HSCs are selectively niche-retained as opposed to stem cells lacking macrophage markers, which exit the BM upon forced mobilization. Macrophage markers on HSCs could be acquired through direct transfer by trogocytosis, regulated by receptor tyrosine-protein kinase C-Kit (CD117), from BM-resident macrophages in mouse and human settings. Our study provides proof of concept that adult stem cells utilize trogocytosis to rapidly establish and activate function-modulating molecular mechanisms.

Hematopoietic stem cells (HSCs) are rare bone marrow (BM) resident cell populations that give rise to all types of blood cells for lifelong tissue maintenance and regeneration (*1*–*3*). Circadian rhythm–controlled molecular oscillations drive the periodical release of a subset of HSCs into circulation (*4*); these periphery-patrolling HSCs confer a key cellular resource for an effective response to and repair of acute as well as chronic hematopoietic tissue injury (*5*, *6*). HSC mobilization can also be pharmacologically induced for therapeutic interventions via modulating cytokine signaling pathways governing stem cell retention in the BM, e.g., through granulocyte colony-stimulating factor (G-CSF) exposure or by inhibiting the interaction between the C-X-C motif chemokine receptor-4 (CXCR4) with its ligand, C-X-C motif chemokine-12 (CXCL12) (*7*, *8*). Autologous and allogeneic transplantation of mobilized HSCs has been a longtime therapeutic mainstay in combating a wide array of degenerative and cancerous diseases, such as inherited, acquired, or cytotoxic therapy–induced bone marrow failure syndromes; immune deficiencies; or hematological malignancies. A large and ever-growing body of work has established molecular and functional heterogeneity of HSC pools as a crucial driver and safeguard of lifelong tissue maintenance, regeneration, and repair (*9*–*15*). Yet, molecular and spatial determinants (e.g., distinct cell surface–presented proteins or proximity of cells to sinusoid blood vessels) of BM egress in a distinct subset of HSCs have been undefined. In this study, we discovered that highly purified HSCs use trogocytosis—a rapid and highly effective mechanism enabling acquisition of membrane-bound proteins from adjacent cells—to license their BM residence and retention.

[1]Ruth L. and David S. Gottesman Institute for Stem Cell and Regenerative Medicine Research, Albert Einstein College of Medicine, Bronx, NY, USA. [2]Department of Cell Biology, Albert Einstein College of Medicine, Bronx, NY, USA. [3]Wisconsin Blood Cancer Research Institute, Department of Pathology and Laboratory Medicine, University of Wisconsin-Madison, Madison, WI, USA. [4]Department of Pathophysiology, Shanghai Jiao Tong University School of Medicine, Shanghai, China. [5]Adult Bone Marrow Transplant Service, Memorial Sloan Kettering Cancer Center, New York, NY, USA. [6]Montefiore-Einstein Comprehensive Cancer Center, Albert Einstein College of Medicine–Montefiore Health System, Bronx, NY, USA. [7]Department of Oncology, Albert Einstein College of Medicine, Bronx, NY, USA. [8]Institute for Aging Studies, Albert Einstein College of Medicine, Bronx, NY, USA.
***Corresponding author. Email: xgao37@wisc.edu (X.G.); britta.will@einsteinmed.edu (B.W.); ulrich.steidl@einsteinmed.edu (U.S.)**
†These authors contributed equally to this work.
‡Present address: AbCellera Biologics, Vancouver, BC, Canada.
§Deceased.

Results

F4/80 presentation on HSCs with attenuated regenerative capacity

We analyzed the phenotypical repertoire of proteins presented on the cell surface of HSCs and their progeny and found F4/80, a canonical macrophage marker (*16*–*18*), on a large fraction (~75%) of highly enriched phenotypical HSCs ($CD150^+$ $Sca\text{-}1^+$ $c\text{-}Kit^+$ $CD34^-$ Lin^-) (Fig. 1A), as well as various multipotent and lineage-committed progenitor populations (fig. S1A). F4/80 expression exhibited a clustered pattern on the surface of these HSCs (Fig. 1B and fig. S1B). Cell-cycle analyses revealed that compared with the pool of stem cells lacking detectable F4/80 presentation, a smaller fraction of F4/80-positive HSCs resided in the G_0 phase of the cell cycle (Fig. 1C), suggesting that the pool of $F4/80^+$ HSCs is less quiescent than their $F4/80^-$ counterparts. To gain insight into the regenerative capacity of $F4/80^+$ and $F4/80^-$ HSC subsets, we carried out serial competitive transplantation experiments of highly sorted HSCs (Fig. 1D). We devised optimized fluorescence-activated cell sorting (FACS), prioritizing purification accuracy and ensuring the highest purity of the isolated HSC to prevent cross-contamination (fig. S1C). Analysis of donor-derived long-term multilineage engraftment 20 weeks after adoptive cell transfer showed a lower total bone marrow chimerism in congenic recipient mice of $F4/80^+$ HSCs compared with mice receiving $F4/80^-$ HSCs, which persisted upon secondary transplantation (Fig. 1E). We found no evidence for a preferential reconstitution of any hematological lineage in recipients of $F4/80^+$ donor HSCs, despite their presentation of a myeloid marker. Donor HSCs from both experimental groups showed balanced multilineage output resulting in comparable relative frequencies of myeloid, B, and T cells within the bulk of donor-derived hematopoietic cells in the peripheral blood of recipient mice (fig. S1, D to F). However, the BM of $F4/80^+$ HSC recipients contained a lower chimerism of donor-derived cells within total HSCs and differentiation-committed progenitor compartments (fig. S1, G and H). We also observed that independent of the F4/80 status, donor HSCs generated both $F4/80^+$ and $F4/80^-$ stem cells, although $F4/80^+$ HSCs were less potent than $F4/80^-$ stem cells in reconstituting the HSC compartment of primary recipient mice overall (fig. S2, A to C). Together, these results suggested that F4/80 cell surface presentation marks a subset of HSCs with attenuated regenerative capacity.

$F4/80^+$ marks an HSC pool refractory to mobilization

Blood cell reconstitution following acute regenerative stress is accompanied by augmented stem cell mobilization to the periphery (*19*). We therefore tested the susceptibility of $F4/80^+$ and $F4/80^-$ HSCs to exit from the bone marrow upon pharmacologically induced mobilization. Compared with vehicle controls, G-CSF robustly mobilized $F4/80^-$ HSCs in the blood; by contrast, $F4/80^+$ HSCs remained in the BM (Fig. 2A and fig. S3A). To assess whether the absence of $F4/80^+$ HSC mobilization was specific to G-CSF stimulation, we administered plerixafor (AMD3100), a CXCR4 antagonist routinely used in the clinic (*20*, *21*). As with G-CSF, plerixafor selectively mobilized $F4/80^-$ but not F4/80-presenting HSCs to the periphery (Fig. 2B), while leaving total HSC numbers in the BM unchanged (fig. S3B). We also assessed the effects of clodronate-mediated depletion of macrophages, which regulate the synthesis of CXCR4 ligand CXCL12 promoting HSC retention in the BM (*22*–*24*); consistently, $F4/80^-$

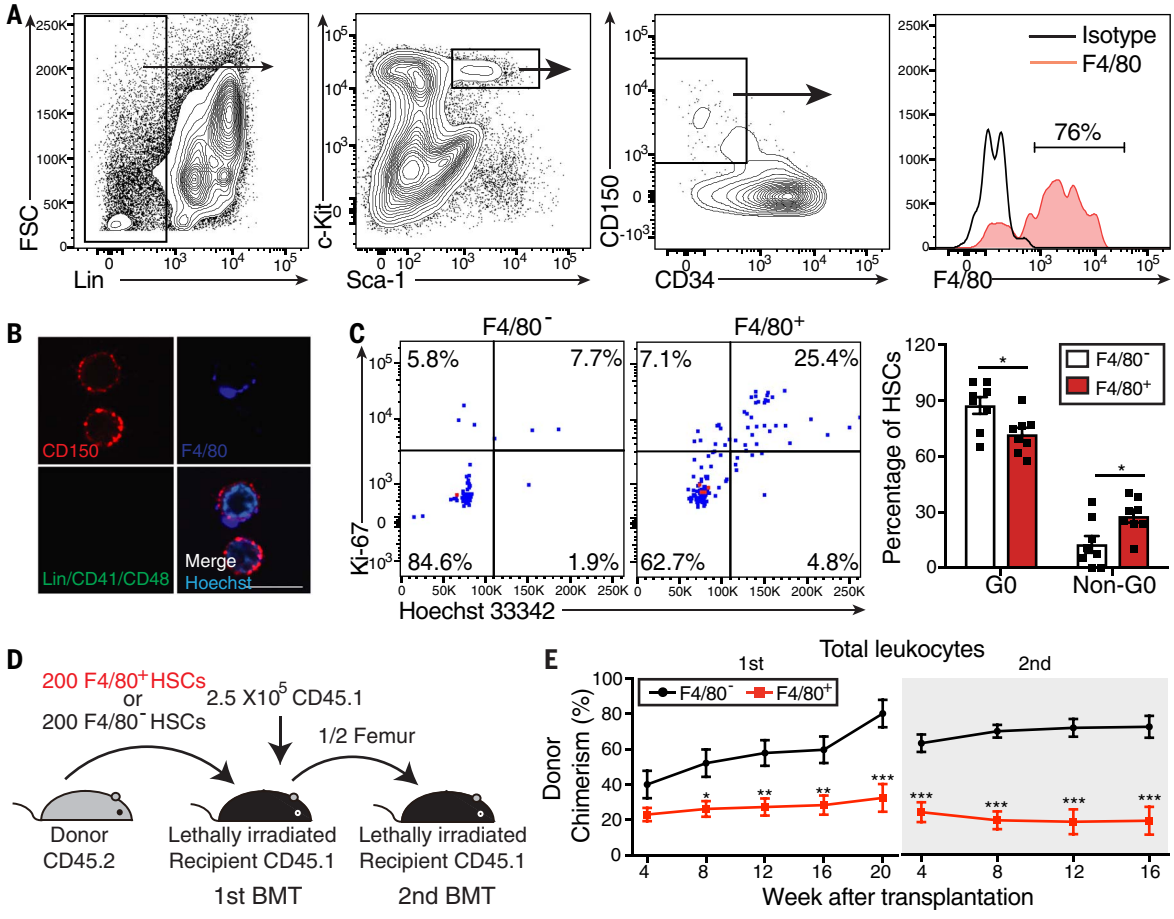

Fig. 1. F4/80 is expressed on hematopoietic stem cells. (**A**) Representative flow cytometry plots showing the percentage of F4/80$^+$ HSCs in total BM HSCs. (**B**) Immunofluorescence images of sorted HSCs stained for F4/80. Scale bar, 10 μm. (**C**) Cell-cycle analyses of HSCs by flow cytometry using anti-K$_i$-67 and Hoechst 33342. Representative plots (left) and quantification (right; each symbol represents a different mouse) are shown; n = 8 mice per group. (**D**) Experimental design for competitive bone marrow transplantation (BMT) of 200 sorted CD45.2 F4/80$^-$ or F4/80$^+$ HSCs along with 250,000 CD45.1 donor cells into lethally irradiated [12 grays (Gy)] CD45.1 mice. For secondary transplantations, bone marrow cells were flushed from femurs of primary recipients and cells from a half femur were transplanted into lethally irradiated CD45.1 mice. (**E**) Donor-derived chimerism (CD45.2$^+$) of total leukocytes from blood of primary (white background) and secondary (gray background) transplanted recipients as shown in (D). n = 7 to 22 mice per group. Data are represented as mean ± SEM and are representative of two (C) or three (E) independent experiments. Statistical significance was assessed by two-way ANOVA with Sidak multiple comparison test [(C) and (E)]. *$P \le 0.05$, **$P \le 0.01$, ***$P \le 0.001$.

HSCs were mobilized to the peripheral blood (Fig. 2C), whereas those expressing F4/80 were retained in BM (fig. S3C). Previous work demonstrated increased peripheral blood mobilization of hematopoietic stem and progenitor cells in mice upon aging (*25*). We next characterized F4/80 presentation in BM HSCs of young (2-month-old) and aged (21-month-old) mice, which uncovered a remarkably lower percentage of F4/80$^+$ HSCs in aged mice (26.4 ± 4.7%) compared with young animals (73.8 ± 3.5%) (Fig. 2D). Consistent with past reports (*26*), we found a sixfold increase in the absolute number of HSCs in the bone marrow. Mobilization of HSCs was enhanced in aged mice (Fig. 2E) and exclusively driven by the F4/80$^-$ HSC fraction (Fig. 2F). These findings demonstrate that F4/80-presenting HSCs are refractory to enforced mobilization to the peripheral blood in young and aged animals. Collectively, our data reveal that mobilizable stem cells lacking the macrophage marker on their cell surface have superior repopulation activity after regenerative stress.

HSCs acquire macrophage-associated markers through cellular transfer

We next sought to gain insight into the functional relevance of and mechanism underpinning F4/80 presentation on HSCs. We wanted to understand whether nonmobilizable HSCs present other macrophage markers, for which we used a genetic model in which the expression of CD169 can be traced by the inducible expression of TdTomato (CD169-Cre;iTdTomato) (*27*). CD169 is an adhesion molecule solely presented on macrophages in the BM and other sites with high monocyte phagocytic activity (*28*). We found that CD169-Cre;iTdTomato labeled a considerable fraction of F4/80$^+$ HSCs (32 ± 8%), in contrast to F4/80$^-$ HSCs, which were largely unlabeled at steady state (2.1 ± 1.2%) (Fig. 2G). Moreover, upon G-CSF–induced HSC mobilization, TdTomato$^+$ HSCs did not egress from the BM (Fig. 2H and fig. S3D), a finding that we recapitulated when using plerixafor-induced HSC mobilization or after macrophage depletion with clodronate liposomes (Fig. 2, I and J, and fig. S3, E and F). The fact that two independent macrophage markers—F4/80 or CD169—labeled a pool of bone marrow–retained HSCs indicated that this property was unlikely to be conferred by the individual receptors.

We next quantified mRNA levels for F4/80-encoding *Adgre1/Emr1* in HSCs, which showed increased mRNA levels in F4/80$^+$ compared with F4/80$^-$ stem cells. Assessment of macrophage scavenger receptor 1 (Msr1/CD204)–encoding *Scara1* (*29*) showed similar expression in F4/80-presenting HSCs and F4/80$^-$ HSCs (fig. S4A), nominating a mechanism other than augmented gene expression as the underlying driver of the observed presentation of at least some macrophage makers. To further test whether BM-resident HSCs expressed these macrophage markers, we utilized reporter mice, allowing for the identification of macrophages through the labeling of cells expressing CD169. We transplanted 200 sorted HSCs from CD169-Cre;iTdTomato$^+$ mice (CD45.2) on the basis of iTdTomato expression (TdTomato$^-$ versus TdTomato$^+$), along with 250,000 donor

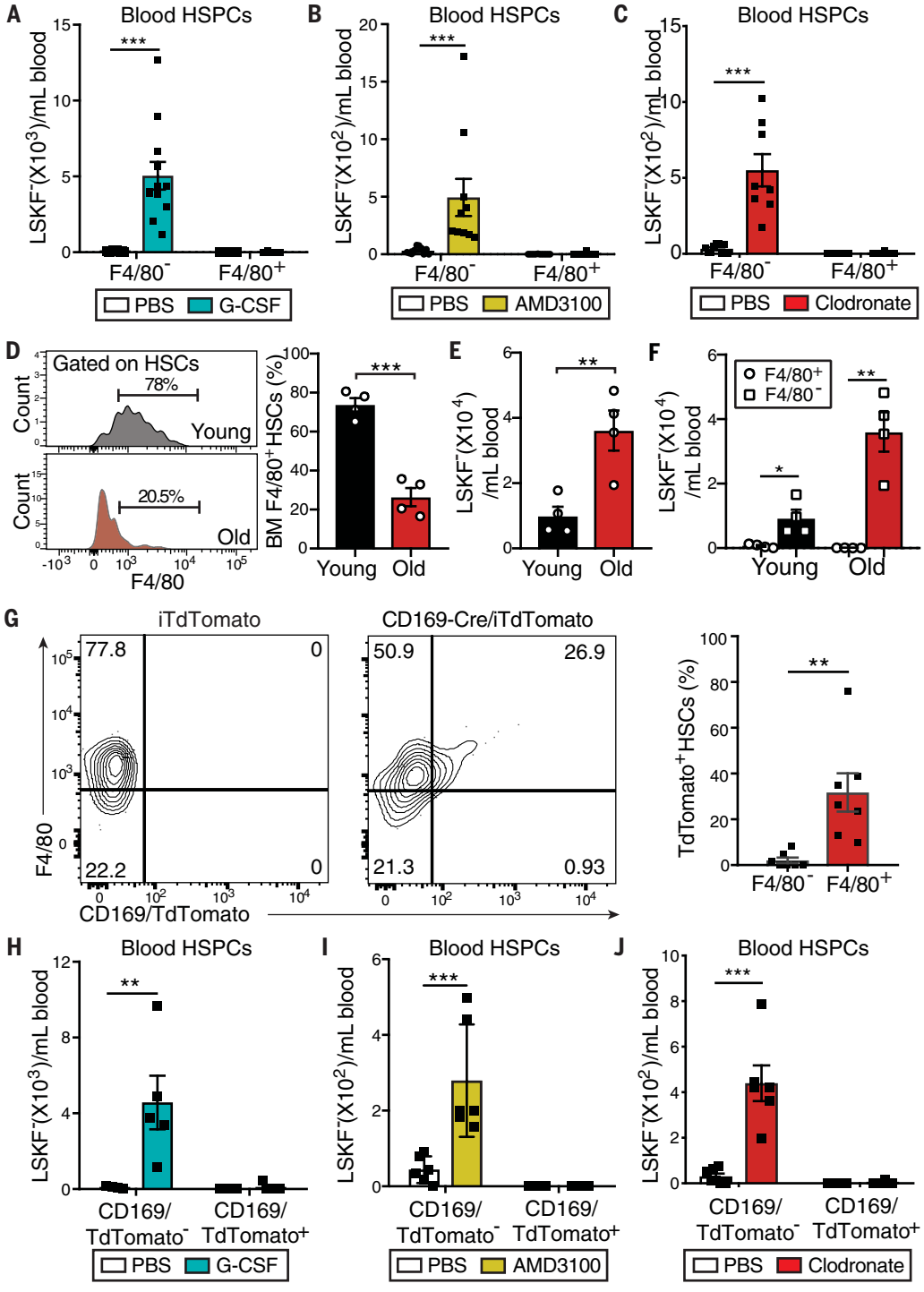

Fig. 2. F4/80⁺ HSC defines a non-mobilizable HSC pool. (**A**) Blood HSPC (LSKF⁻: Lin⁻ Sca-1⁺ c-Kit⁺ Flt3⁻) numbers after PBS or G-CSF treatment; *n* = 11 to 12 mice. (**B**) Blood LSKF⁻ numbers after PBS or AMD3100 (5 mg/kg) treatment; *n* = 10 to 11 mice. (**C**) Blood LSKF⁻ numbers after PBS or clodronate liposomes treatment; *n* = 10 to 11 mice. (**D**) (Left) Representative flow cytometry plots and (right) percentage of F4/80⁺ HSCs in the bone marrow in young and old mice; *n* = 4 mice (**E**) Blood HSPC (LSKF⁻: Lin⁻ Sca-1⁺ c-Kit⁺ Flt3⁻) numbers in young and old mice; *n* = 4 mice. (**F**) Blood F4/80⁺ and F4/80⁻ HSPC numbers in young and old mice; *n* = 4 mice. (**G**) (Left) Representative flow cytometry plots showing F4/80 and TdTomato expression in bone marrow HSCs from iTdTomato and CD169-Cre/iTdTomato mice. (Right) Percentage of TdTomato⁺ HSCs in F4/80⁻ and F4/80⁺ HSCs from CD169-Cre/iTdTomato mice. *n* = 7 mice. (**H** to **J**) Blood LSKF⁻ numbers after (E) PBS or G-CSF treatment in CD169-Cre/iTdTomato mice; *n* = 4 to 5 mice; (F) PBS or AMD3100 (5 mg/kg) treatment in CD169-Cre/iTdTomato mice, *n* = 6 mice; and (G) clodronate liposomes treatment in CD169-Cre/iTdTomato mice; *n* = 6 to 7 mice. Data in (A) to (J) are represented as mean ± SEM and are representative of two independent experiments; each symbol represents a different mouse. Statistical significance was assessed using two-way ANOVA with Sidak multiple comparisons test [(A) to (C) and (H) to (J)] or two-tailed unpaired *t* test [(D) to (G)]. **P* ≤ 0.05, ***P* ≤ 0.01, ****P* ≤ 0.001.

BM cells (CD45.1), into lethally irradiated CD45.1 congenic mice (Fig. 3A). If CD169 was transcribed and translated in HSCs, one would expect detection of TdTomato expression in the HSC progeny. However, we found that the percentage of TdTomato⁺ HSCs was higher in animals transplanted with TdTomato⁻ HSCs, suggesting that CD169 (along with F4/80) was acquired rather than expressed within HSCs (Fig. 3B). To confirm the extrinsic origin of CD169 expression, we transplanted whole BM cells from CD45.1 congenic mice (that do not express TdTomato) into lethally irradiated CD169-Cre;iTdTomato recipients and determined whether TdTomato could be transferred from recipient-derived macrophages to donor-derived HSCs (Fig. 3C). Analysis of donor HSCs at 16 weeks posttransplantation revealed that the TdTomato signal was detected in donor F4/80⁺ CD45.1 HSCs (Fig. 3D). Confocal microscopy showed that the TdTomato signal was almost exclusively located on the cell membrane (Fig. 3E). This set of data shows that macrophage markers, including F4/80 and CD169, can be acquired by cellular transfer.

Transfer of BM-retention machinery from macrophages to stem cells

Next, we set out to pinpoint the mechanism driving enhanced BM retention of macrophage marker–presenting HSCs. BM-resident macrophages express levels of CXCR4—a chemokine receptor required to retain HSC in bone marrow

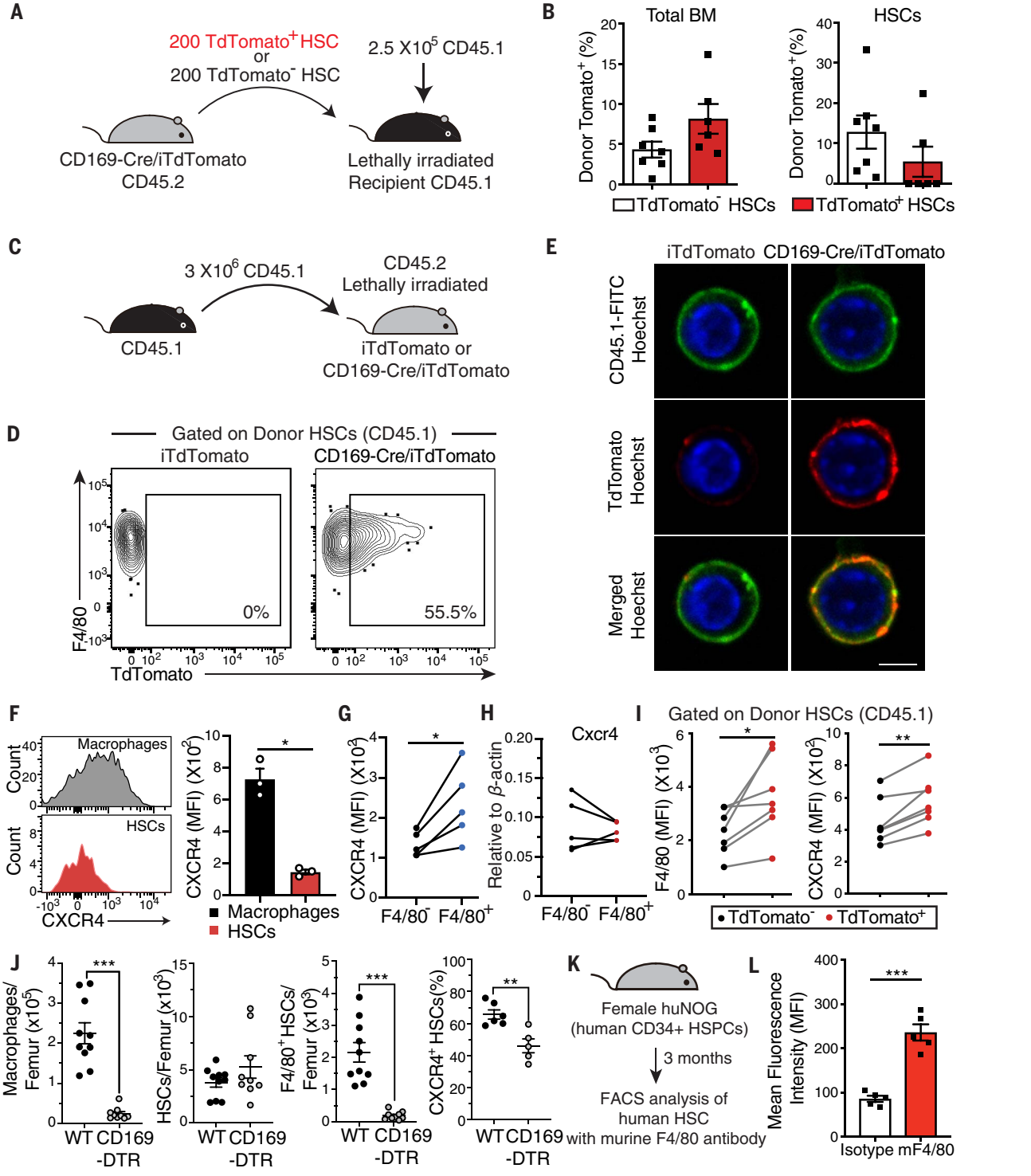

Fig. 3. HSCs acquire membrane signaling components from BM macrophages, thereby enhancing CXCR4-mediated anchoring in bone marrow. (**A**) Experimental design for competitive transplantation of 200 sorted TdTomato$^-$ or TdTomato$^+$ from CD169-Cre/iTdTomato mice (CD45.2) with 250,000 CD45.1 cells into lethally irradiated (12 Gy) CD45.1 recipients. (**B**) TdTomato expression in total BM (left) and BM HSCs (right) in mice transplanted with TdTomato$^-$ or TdTomato$^+$ HSCs; n = 6 to 7 mice. (**C**) Experimental design for noncompetitive BM transplantation of 3 × 10^6 cells from CD45.1 C57BL/6 mice into lethally irradiated iTdTomato control mice or CD169-Cre/iTdTomato mice (CD45.2). (**D**) Representative plots of TdTomato expression in BM donor HSCs from control iTdTomato or CD169-Cre/iTdTomato mice transplanted as shown in (C). (**E**) Representative confocal images showing localization of the TdTomato signal on the cell membrane. Scale bar, 10 μm. (**F**) Representative flow cytometry plots and quantification of mean fluorescence intensities (MFI) in CXCR4 expression on BM macrophages (Gr-1$^-$ F4/80$^+$ CD115^{int} SSC$^{int/lo}$) and HSCs (Lin$^-$ Sca-1$^+$ c-Kit$^+$ CD150$^+$ CD34$^-$); n = 3 mice. (**G**) Quantification of MFI in CXCR4 expression on F4/80$^-$ and F4/80$^+$ HSCs; n = 5 mice. (**H**) Quantification of *Cxcr4* mRNA levels in sorted F4/80$^+$ and F4/80$^-$ HSCs from the bone marrow by quantitative reverse transcription polymerase chain reaction; n = 5 biological replicates. (**I**) Expression of F4/80

and CXCR4 within BM donor TdTomato$^-$ and TdTomato$^+$ HSCs from CD169-Cre/iTdTomato recipients; n = 7 mice. (**J**) The number of macrophages, HSCs, and F4/80$^+$ HSCs per femur and the percentage of CXCR4$^+$ HSCs in the bone marrow from WT and CD169-DTR mice following DT treatment; n = 5 to 10 mice per group. (**K**) Experimental design to test F4/80 transfer from mouse macrophages to human HSCs in vivo in immunodeficient huNOG mice transplanted with human CD34$^+$ HSPCs. (**L**) MFI of mouse F4/80 signal on human HSCs; n = 5 mice. Data are represented as mean ± SEM and are representative of two [(B), (F) to (I), and (L)] or three (J) independent experiments; each data point represents a different mouse. Statistical significance was assessed using two-tailed paired t test [(F) to (I); paired dots are connected by lines in (G) to (I)] or two-tailed unpaired t test [(B), (J), and (L)]. *$P \leq 0.05$, **$P \leq 0.01$, ***$P \leq 0.001$.

(*30*)—that are 4.9 times as high as those found in HSCs (Fig. 3F). In support, we found that F4/80$^+$ HSCs showed more CXCR4 on their cell surface than did F4/80$^-$ HSCs (Fig. 3G), although their mRNA levels of *Cxcr4* were undistinguishable (Fig. 3H). Moreover, in CD169-Cre;iTdTomato mice (CD45.2) engrafted with CD45.1$^+$ HSCs, we also detected higher F4/80 and CXCR4 levels on donor-derived (CD45.1) TdTomato$^+$ HSCs compared with TdTomato$^-$ HSC (Fig. 3I). We next probed whether the acquisition of CXCR4 played a functional role and predicted that F4/80$^+$ HSCs show an increased ability to respond to CXCR4 ligand CXCL12 (*7*). Indeed, compared with F4/80$^-$ HSCs, F4/80-presenting stem cells were more responsive to a gradient of CXCL12, showing enhanced migratory capacity in transwell assays (fig. S4B). We also found evidence for the activation of CXCR4-associated receptor signaling (*31*) in F4/80$^+$ HSCs after CXCL12 exposure, which led to a 4.7-fold increase of phosphorylated extracellular signal–regulated kinase (ERK) 1/2 compared with F4/80$^-$ counterparts (fig. S4B). To test the possibility that F4/80$^+$ stem cells reside in a mobilization-favoring location in the BM, we used in vivo confocal immunofluorescence microscopy (*32*). This showed F4/80$^-$ and F4/80$^+$ HSCs at similar distance to sinusoids, with 86.3 ± 6.7% of F4/80$^-$ and 85 ± 7.6% F4/80$^+$ located within a 20-μm distance from sinusoids, respectively (fig. S4C), rendering the possibility of a mobilization-supportive microenvironment for F4/80$^+$ HSCs rather unlikely. Collectively, these results suggested that cellular transfer of CXCR4 along with macrophage markers to a subset of HSCs acts as one of the mechanisms to confer stem cell residence in the BM.

To test BM macrophages as the cellular source of HSC-transferred F4/80 and CXCR4, we used a gold-standard genetic model for the depletion of macrophages, which expresses the diphtheria toxin receptor (DTR) under the endogenous promoter driving the expression of CD169-encoding *Siglec1* (CD169-DTR) (*33*). Our previous work demonstrated that CD169-presenting macrophages in close proximity to HSCs are critical for maintaining stem cell residency in the BM (*22*). Treatment of CD169-DTR mice with DT depleted CD169$^+$ macrophages by 90% compared with DT-treated wild type (WT) control mice (Fig. 3J). Flow cytometric analysis revealed that macrophage depletion reduced F4/80$^+$ and CXCR4$^+$ HSCs without affecting the total number of HSCs in the BM (Fig. 3J), implicating CD169$^+$ macrophages as a cellular source of HSC-transferred membrane proteins. To corroborate membrane transfer between macrophages and HSCs, we used Dil-labeled liposomes (fig. S4D), which are selectively ingested by mononuclear phagocytes (*34*). Flow cytometry and immunofluorescence analyses revealed Dil fluorescence in BM HSCs (as well as in other hematopoietic progenitor cell populations, although at lower levels) from UBC-GFP mice [transgenic mice expressing green fluorescent protein (GFP) under the control of the human ubiquitin C (UBC) promoter] receiving Dil-liposomes (fig. S4, E and F). Dil-liposome incorporation was much higher in F4/80$^+$ HSCs compared with F4/80$^-$ controls (fig. S4, G to I), confirming the cellular transfer from macrophages to HSCs. To evaluate whether such membrane transfer also occurred in human HSCs, we performed xenotransplantation of CD34-enriched human hematopoietic stem and progenitor cell (HSPC) specimens (CD34 is a known marker for human HSPCs) into nonobese diabetic (NOD)/Shi-scid/interleukin-2 (IL-2)Rγ–null mice. As host BM macrophages persist after transplantation (*35*), we tested whether mouse-specific F4/80 could be found on engrafted human CD34$^+$ cells (Fig. 3K) and indeed detected mouse F4/80 on xenografted human HSPCs (Fig. 3L and fig. S4J). Together, these findings uncovered transfer of CXCR4 from macrophages to stem cells in both mice and humans.

Transfer from macrophages to HSCs is mediated by trogocytosis

Cells use various mechanisms to transfer cellular components. We obtained TdTomato$^+$ BM-derived macrophages from Rosa$^{mT/mG}$ transgenic mice that express membrane-targeted TdTomato (mTdTomato) before Cre-mediated excision (*36*) and performed cocultures with lineage-depleted (Lin$^-$) BM cells from UBC-GFP mice (*37*). We tested whether extracellular vesicles were involved in the transfer between macrophages and HSCs. We collected supernatant from macrophage cultures and found that GFP$^+$ HSCs cultured in the supernatant showed no mTdTomato signal (fig. S5A). Additionally, we found that treatment with an exosome inhibitor (GW4869) did not affect the transfer from macrophages to HSCs compared with dimethyl sulfoxide control treatment (fig. S5B), thereby excluding the possibility that exosome formation was required for the transfer between macrophages and HSCs. However, the transfer of mTdTomato from macrophages to HSCs seemed to be an active cellular process, as coculture at 4°C suppressed the transfer as compared with the effect at 37°C (fig. S5C).

We next investigated whether direct cell-to-cell contact between macrophages and HSCs was required by using transwell cultures (Fig. 4A). We found that GFP$^+$ HSCs cultured in the presence of mTdTomato$^+$ BM macrophages acquired mTdTomato (63% GFP$^+$ mTdTomato$^+$; Fig. 4A). Transwell experiments revealed that cell-cell interaction was critical because the separation of GFP$^+$ cells and mTdTomato$^+$ macrophages abolished the transfer (Fig. 4A). Confocal microscopy revealed plasma membrane translocation of mTdTomato$^+$ BM-derived macrophages to GFP$^+$ lineage-depleted BM cells (Fig. 4B and fig. S5D). These data revealed that HSCs acquired membrane material from macrophages, which necessitates a direct cell-cell interaction. A time-course analysis revealed that the transfer occurred rapidly, because the transfer peaked 5 min after coculture (Fig. 4C). The rapidity of the process and requirement of cell contact was consistent with trogocytosis, an actin-dependent transfer mechanism mostly described in immune cells (*38*–*40*). In line with these results, cytochalasin D, an actin polymerization inhibitor, impaired mTdTomato transfer from macrophages to GFP$^+$ Lin$^-$ cells (Fig. 4D and fig. S5E). We also found that mTdTomato$^+$ HSCs exhibited higher levels of CXCR4 compared with mTdTomato$^-$ HSCs after coculture (Fig. 4E). Together, these findings implicate trogocytosis as a key mechanism for licensing BM retention in HSCs.

C-Kit regulates HSC trogocytosis

In the course of our experiments, we discovered that trogocytosis was impaired when stem cell factor (SCF) was added to the media of HSC and macrophage cocultures (fig. S5F). SCF is a well-established ligand of receptor tyrosine-protein kinase c-Kit (CD117) and an essential hematopoietic growth factor required for HSC maintenance (*41*). To examine the functional role of c-Kit signaling in macrophage membrane transfer, we exposed HSCs in macrophage cocultures to pan-tyrosine kinase inhibitor imatinib (*42*), which suppressed trogocytosis (Fig. 4F and fig. S5G). Treatment of mice with imatinib also led to impaired F4/80 presentation on stem cell–enriched Lin$^-$ Sca1$^+$ cKit$^+$ (LSK) cell populations (fig. S5H). We next examined c-Kit–specific receptor inhibition using ligand engagement–mediated receptor internalization (*43*). We exposed freshly sorted HSCs to increasing concentrations of

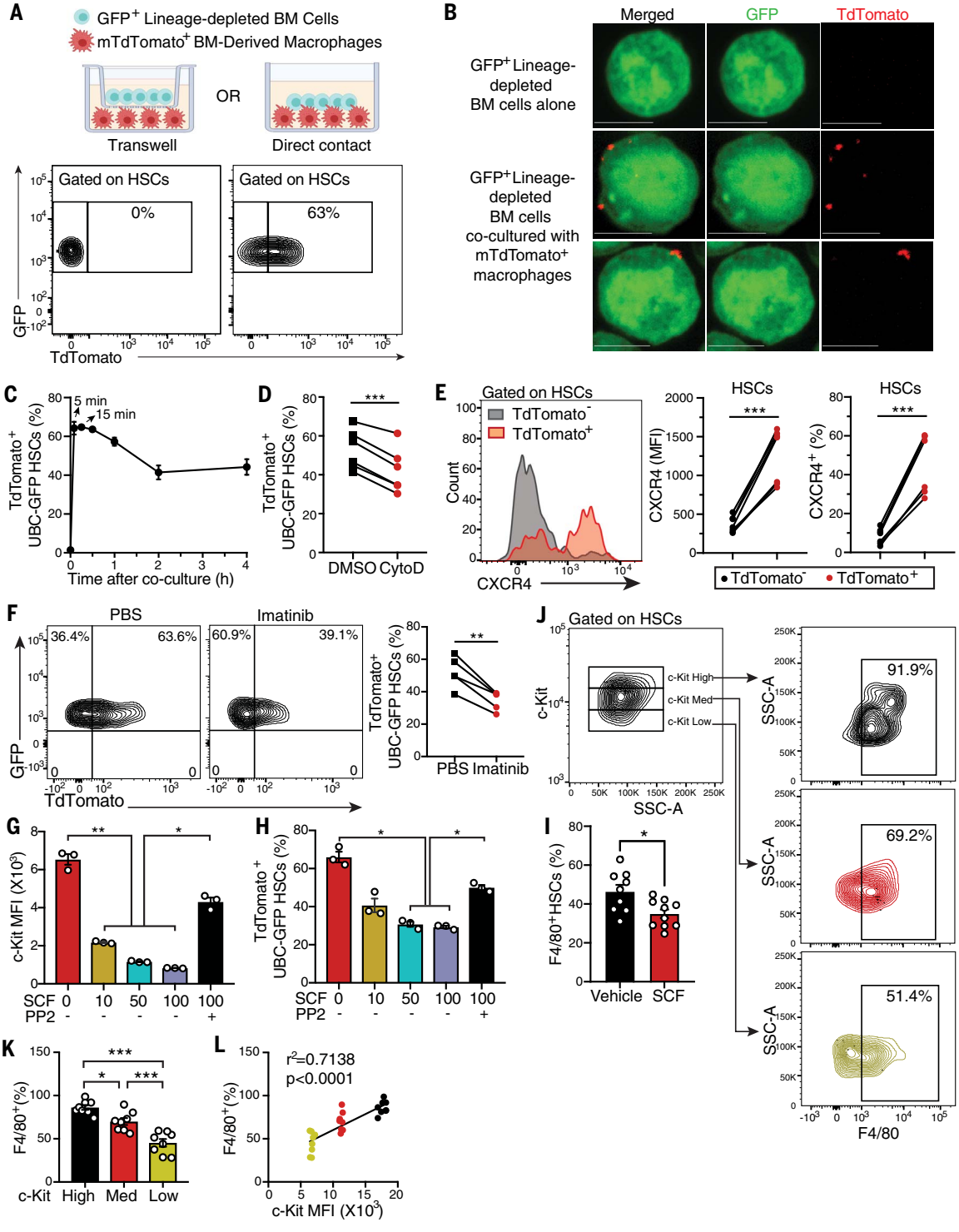

Fig. 4. HSCs acquire membrane signaling components from BM macrophages through c-Kit–mediated trogocytosis. (**A**) Transwell (no direct cell contact) and coculture (direct-contact) experiments in which TdTomato$^+$ BM macrophages (from Rosa$^{mT/mG}$ mice) were incubated in the presence of GFP$^+$ lineage-depleted BM cells (from UBC-GFP mice). Flow plots show the percentage of TdTomato$^+$ GFP$^+$ HSCs in total HSCs (defined by Lin$^-$ Sca-1$^+$ c-Kit$^+$ CD150$^+$ CD34$^-$) in transwell or direct-contact setting. (**B**) Representative confocal images showing plasma membrane transfer from TdTomato$^+$ BM-derived macrophages to GFP$^+$ lineage-depleted BM cells. GFP$^+$ lineage-depleted BM cells were cocultured with or without TdTomato$^+$ macrophages for 1 hour and then taken out for cytospin before confocal microscopy analysis. Scale bar, 5 μm. (**C**) Time course of percentage of TdTomato$^+$ GFP$^+$ HSCs after coculture for 5, 15, 30, 60, 120, and 240 min; n = 4 biological replicates (**D**) Percentage of TdTomato$^+$ GFP$^+$ double-positive HSCs after coculturing of GFP$^+$ lineage-depleted cells with TdTomato$^+$ macrophages in the presence of actin depolymerizing agent cytochalasin D; n = 6 biological replicates. (**E**) MFI of CXCR4 on TdTomato$^-$ and TdTomato$^+$ HSCs and percentage of CXCR4$^+$ HSCs within TdTomato$^-$ and TdTomato$^+$ HSCs; n = 7 biological replicates. (**F**) Representative flow cytometry plots and percentage of TdTomato$^+$ GFP$^+$ double-positive HSCs after coculturing of GFP$^+$ lineage-depleted cells with TdTomato$^+$ macrophages with PBS or imatinib; n = 5 biological replicates. (**G** and **H**) MFI of c-Kit signal on BM HSCs (G) and percentage of TdTomato$^+$ GFP$^+$ double-positive cells after coculturing of TdTomato$^+$ BM macrophages with GFP$^+$ lineage-depleted BM cells in the presence of 0, 10, 50, 100 ng/ml SCF (with or without PP2 treatment) (H); n = 3 biological replicates. (**I**) Percentage of F4/80$^+$ HSCs in the bone marrow with vehicle or SCF treatment; n = 9 to 10 mice per group. (**J** to **L**) Percentage of F4/80$^+$ HSCs in the c-Kit^{high}, c-Kit^{med}, and c-Kit^{low} HSC populations; n = 8 mice. Data in (C) to (L) are represented as mean ± SEM and are representative of two independent experiments; each symbol represents a different biological sample [(D) to (H)] or mouse [(I), (K), and (L)]. SSC, skeletal stem cell. Statistical significance was assessed using two-tailed paired t test [(D) to (F); paired dots are connected by lines] or two-tailed unpaired t test (I) or one-way ANOVA with Tukey's multiple comparisons test [(G), (H), and (K)] or Ozone correlations (L). *$P \le 0.05$, **$P \le 0.01$, ***$P \le 0.001$.

SCF, which showed an inverse dose-response relationship between SCF abundance and c-Kit expression; high doses of SCF were also associated with the lowest mTdTomato transfer (Fig. 4, G and H). Specific c-Kit down-regulation can also be achieved by the activation of Src kinase, which phosphorylates c-Cbl E3 ubiquitin ligase that promotes c-Kit degradation (*44*, *45*). We observed that treatment with a Src inhibitor (PP2), which decreases c-Cbl phosphorylation (*45*), also rescued c-Kit expression on HSCs and transfer of mTdTomato (Fig. 4, G and H). Furthermore, in vivo administration of SCF impaired transfer of F4/80 from macrophages to BM HSCs in mice (Fig. 4I). In the unperturbed state, we found a strong positive correlation between c-Kit and F4/80 expression on BM HSCs (Fig. 4, J-L). Consistently, in vitro trogocytic activity was strongly correlated with c-Kit presentation on HSCs (fig. S5I). Moreover, in comparison with young HSCs, aged stem cells showed reduced c-Kit expression (fig. S5J), which is consistent with attenuated macrophage transfer and enhanced mobilization of HSCs during aging (Fig. 2, H to J). RNA-sequencing analysis of F4/80$^+$ and F4/80$^-$ HSCs additionally revealed that the top up-regulated pathway in F4/80$^+$ HSCs is associated with Rho signaling (fig. S5, K and L)—an important downstream pathway of both CXCR4 and c-Kit—required for CXCL12/CXCR4-induced migration (*46*). Together, these data strongly implicated c-Kit in the regulation of HSC trogocytosis.

Lastly, we evaluated the functional relevance of our findings to human hematopoiesis. We determined whether macrophage markers were present on human hematopoietic stem cells (hHSCs). As the expression of the human ortholog of F4/80, EMR1, is limited to eosinophils (*47*), we focused on other human macrophage markers. We found that a considerable number of BM-derived hHSCs (CD34$^+$, CD38$^-$, CD90$^+$, CD45RA$^-$, and CD49f$^+$) presented macrophage markers CD11b (60.0%), CD14 (66.8%), or CD163 (50.4%) (Fig. 5, A to C). Moreover, the fraction of macrophage marker–presenting hHSCs was higher in BM-derived specimens than in samples from mobilized human peripheral blood (PB) (Fig. 5D); analysis of paired human PB and BM samples further validated this observation (Fig. 5E). We next determined whether hHSCs relied on C-Kit for macrophage trogocytosis. In support of this idea, we found a higher fraction of CD11b-presenting cells within hHSCs with high C-Kit presentation (C-Kit^{high}) compared with hHSCs expressing lower amounts of the receptor (C-Kit^{low}) (Fig. 5F). We obtained similar results using CD14 and CD163 (Fig. 5, G and H), which are consistent with our findings made in mouse models. To ascertain that macrophage marker–presenting hHSCs harbored hematopoietic reconstitution ability, we performed transplantation experiments, which demonstrated that macrophage marker-presenting hHSCs are capable of lymphoid and myeloid repopulation (fig. S5M).

Discussion

Our results demonstrate that trogocytosis by a stem cell can alter its behavior. Indeed, only HSCs that have not undergone trogocytosis can be mobilized to the peripheral blood. Our data suggest that constitutive trogocytic activity of HSCs is a common and regulated event. Moreover, our data suggest that c-Kit is a critical pathway regulating HSC trogocytosis. High c-Kit expression and signaling is linked to high trogocytic activity and BM retention. Moreover, our data suggest that mobilization itself enriches for HSCs with high self-renewal potential; we found reduced repopulation activity of highly c-Kit–expressing F4/80$^+$ HSCs (c-Kit^{high}), which is consistent with a recent report suggesting that c-Kit^{high} HSCs exhibit lower self-renewal potential compared with c-Kit^{low} HSCs (*48*). Our results also provide a mechanistic explanation for the observation that mobilized hHSCs present less C-Kit than their BM counterparts (*49*), and for the synergistic effect of recombinant C-Kit ligand (SCF) to enhance G-CSF–induced HSC mobilization (*50*). Further studies are needed to investigate the precise mechanisms underlying SCF-enhanced stem cell mobilization and to leverage these insights for clinical application.

Our results also revealed a previously unappreciated function for BM-resident macrophages in the HSC niche. Bone marrow ("central") CD169$^+$ macrophages interact closely with red blood cell precursors to form erythroblastic islands (*51*, *52*); they can also secrete factors [e.g., oncostatin M (*53*)] and regulate CXCL12 expression by mesenchymal stromal cells (*22*–*24*). The present results suggest a more intimate relationship of resident macrophages with HSCs, whereby the macrophage, through direct cell-to-cell contact, could control HSC behavior. It will be interesting to further examine the precise dynamics of trogocytosis-mediated transfer from macrophages to HSCs in future studies through in vivo imaging using emerging technologies (*54*). Our results show that macrophages can assign BM residence through the supply of membrane-anchored CXCR4 and probably other macrophage-derived anchoring mechanisms. It will also be interesting to further study the functional role of CXCR4 transfer in vivo. The potential relevance of the latter is suggested because treatment with plerixafor, a CXCR4 antagonist, also exclusively mobilized F4/80$^-$ HSPCs. Mobilized HSCs in the peripheral blood are a major source for hematopoietic stem cell transplantation therapies for patients with cancer, autoimmune, and other disorders. As patients with a limited marrow reserve (e.g., because of the disease process itself or prior treatment) often fail to mobilize HSPC efficiently (*55*), a greater understanding of macrophage-HSC transfer may provide approaches to increase the mobilized HSC yield.

Materials and methods

Animals

CD169-Cre and CD169-DTR mice were a gift from Masato Tanaka (Tokyo University of Pharmacy and Life Sciences). B6.Cg-Gt(ROSA)26Sor$^{tm14(CAG–tdTomato)Hze}$/J (iTdTomato), B6. 129(Cg)-Gt(ROSA)26Sor$^{tm4(ACTB-tdTomato,-EGFP)Luo}$/J (Rosa26mT/mG), C57BL/6-Tg(UBC-GFP)30Scha/J, and C57BL/6-CD45.1/2 congenic strains were purchased from Jackson Laboratory. All experiments, unless otherwise noted, were performed on 9-to-13-week-old mice of both genders. No statistical method was used to predetermine sample size and sample size was chosen based on previous studies performed in our lab. Mice were randomly assigned to experimental groups including male and female mice. All mice were maintained in pathogen-free conditions under a 12:12-hours light/dark cycle and fed with PicoLab Rodent Diet 20 (5053) ad libitum. Animals were euthanized via CO_2 asphyxiation or cervical dislocation under anesthesia. This study complied with all ethical regulations involving experiments with mice, and all experimental procedures performed on mice were approved by the Institutional Animal Care and Use Committee (IACUC) of Albert Einstein College of Medicine (protocols: 00001230, 20180901, 00001101, and 00001372).

In vivo treatments

G-CSF was administered subcutaneously (s.c.) at a dose of 125 μg/kg twice a day (eight divided doses) beginning in the evening of the first day and blood was harvested 3 hours after the final morning dose of G-CSF. For plerixafor-induced mobilization, mice received a single dose of plerixafor (5 mg/kg) intraperitoneally (i.p.) 1 hour before blood collection. Clodronate liposomes or phosphate-buffered saline (PBS) liposome as control (250 μl) were infused i.v. 14 hours before analysis to deplete mononuclear phagocytes. CD169-DTR or control mice were injected i.p. with 10 μg/kg DT 48 hours before harvest. SCF was injected s.c. at 25 μg/kg twice a day (eight divided doses).

Bone marrow transplantation

In competitive HSC repopulation assays, 200 donor F4/80$^{+/-}$ or TdTomato$^{+/-}$ HSCs (Lin$^-$ Sca-1$^+$ c-Kit$^+$ CD34$^-$ CD150$^+$) were sorted from C57BL/6 mice (CD45.2) or CD169-Cre;iTdTomato, respectively, and injected into lethally irradiated (12 Gy) recipient mice (CD45.1) in combination with 250,000 bone marrow cells (CD45.1). For secondary bone marrow transplantation, half of the bone marrow cells from a femur from primary recipient chimeric mice were transplanted into

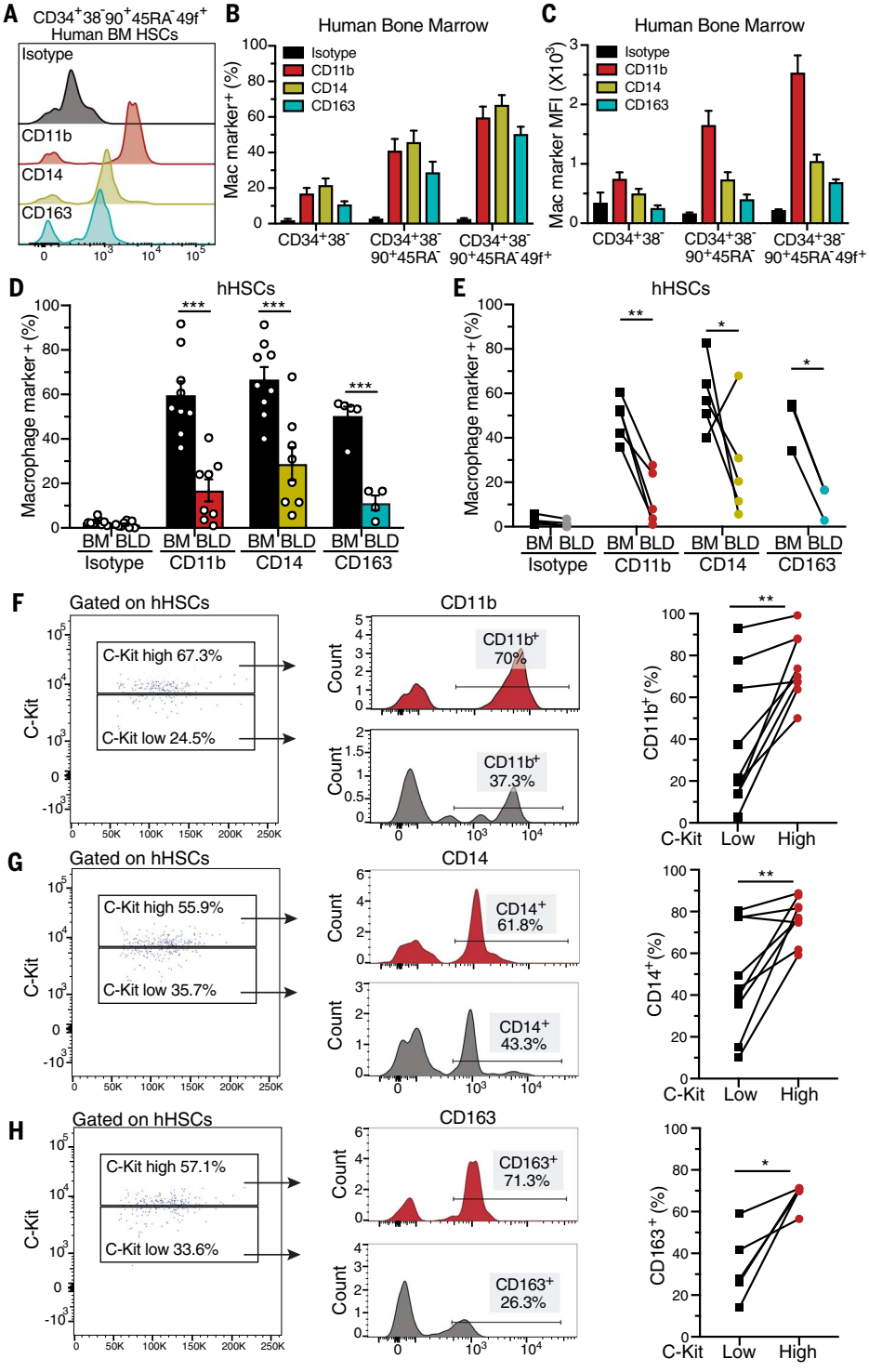

Fig. 5. Macrophage markers are present on human HSCs. (**A**) Representative flow plot showing that human BM HSCs ($CD34^+$ $CD38^-$ $CD90^+$ $CD45RA^-$ $CD49f^+$) stained positive for macrophage markers, CD11b, CD14, and CD163. (**B** and **C**) Quantification of macrophage markers on human hematopoietic stem and progenitor populations in the BM; *n* = 9, 9, 9, and 5 biological replicates for isotype, CD11b, CD14, and CD163, respectively. (**D**) Quantification of macrophage markers on human BM HSCs and PB HSCs; *n* = 9, 9, 9, and 5 biological replicates for isotype, CD11b, CD14, and CD163, respectively. (**E**) Quantification of macrophage markers on HSCs from paired BM and PB samples; *n* = 5, 5, 5, and 3 biological replicates for isotype, CD11b, CD14, and CD163, respectively. (**F** to **H**) Percentage of $CD11b^+$ (F), $CD14^+$(G), and $CD163^+$ (H) HSCs within the C-Kit^{low} and C-Kit^{high} HSC populations in human bone marrow samples; *n* = 9, 9, and 5 biological replicates for (F), (G), and (H), respectively. Data are represented as mean ± SEM and are representative of five (E) or nine [(B) to (D) and (F) to (H)] independent experiments; each symbol represents a different biological sample. Statistical significance was assessed using two-tailed paired *t* test [(E) to (H); paired dots are connected by lines] or two-tailed unpaired *t* test (D). $^*P \le 0.05$, $^{**}P \le 0.01$, $^{***}P \le 0.001$.

lethally irradiated (12 Gy) recipients (CD45.1). CD45.1/CD45.2 chimerism of recipient blood and bone marrow was analyzed up to 20 weeks after transplantation using FACS analysis. Whole bone marrow transplantation was performed by harvesting bone marrow cells from C57BL/6 mice (CD45.1) and transplanting 3×10^6 cells into each lethally irradiated (12 Gy) iTdTomato or CD169-Cre/iTdTomato mice (CD45.2).

Cell-cycle analysis

BM cells were stained with surface markers, fixed, and permeabilized using BD Cytofix/CytopermTM Fixation/Permeabilization Kit according to the manufacturer's protocol, and stained with anti-Ki67 antibody and Hoechst 33342 at 20 mg/ml for 30 min. After washing, cells were analyzed by LSRII Flow Cytometer (Becton Dickinson).

Cell culture assays

To culture bone marrow–derived macrophages (BMDM), femurs, tibias, humeri, and pelvic bones from Rosa26mTmG mice were flushed by 1 ml of syringe with a 21-gauge needle into sterile PBS (Corning) and all bone marrow cells were plated into non-treated tissue culture dishes containing macrophage culture media (RPMI1640 w/Glutamine + 10% FBS + 1% P/S +

10 mM HEPES + 10 ng/ml CSF1). After 3 days, 5 ml of BMDM media was added in each 10-cm petri dish. After 5 days, cells were washed twice with PBS and fresh new BMDM media was added. After 7 days, BMDM adhered to the bottom were washed with PBS, trypsinized and resuspended in BMDM media for transwell or coculture assay. For transwell or coculture experiments, femurs, tibias, humeri, and pelvic bones from UBC-GFP mice were flushed using 1 ml sterile phosphate-buffered saline (PBS, Corning) with a 21-gauge needle, erythrocytes were lysed, and lineage-positive cells were immunomagnetically depleted using a biotinylated lineage antibody cocktail (CD3e, B220, CD11b, Ter119, and Gr-1, at 1:100 dilution) (BD Bioscience 559971) and subsequent streptavidin magnetic beads (Miltenyi Biotech 130-48-101). Lineage-depleted UBC-GFP cells were transferred into the bottom of transwells filled with media containing RPMI1640 supplemented with 10% FBS, 1% P/S, 1% L-glutamine, 10 mM HEPES, 25 nM TPO, and 25 nM SCF (where indicated). BMDM were transferred into the transwells for non-direct contact culture or into the bottom for direct contact coculture. For coculture with inhibitors, TdTomato$^+$ macrophages and GFP$^+$ lineage-depleted bone marrow cells were pretreated with 50 μM of Cytochalasin D (Sigma-Aldrich), 10 μM of imatinib (Sigma-Aldrich), or 1 μM of GW4869 (Sigma-Aldrich) for 1 hour, and then cocultured in the presence of 50 μM of Cytochalasin D, 10 μM of imatinib, or 1 μM of GW4869 for another 2 hours before analysis.

Flow cytometry and sorting

Peripheral blood was harvested by retro-orbital bleeding of mice anesthetized with isoflurane and collected in polypropylene tubes containing EDTA. Blood parameters were determined with the Advia 120 Hematology System (Siemens). BM cells were obtained by flushing and dissociating with 1 ml PBS in a syringe with a 21-gauge needle. For FACS analysis or sorting of hematopoietic cell populations, RBCs were lysed and washed in ice-cold PEB (PBS containing 0.5% BSA and 2 mM EDTA) before staining with antibodies in PEB. The following antibodies were used for flow cytometry: the anti-lineage panel cocktail (CD3e, B220, CD11b, Ter119, and Gr-1, at 1:50 dilution) was from BD Bioscience (559971), anti-Sca-1-AF700 (D7, 108142), anti-CD117(c-Kit)-PE/Cy7 (2B8; 105814), anti-CD34 Biotin (RAM34, 13-0341-85), anti-CD150-BV421 (TC15-12F12.2, 115925), anti-F4/80-BV650 (BM8, 123149), anti-CXCR4-AF647 (L276F12, 146504), anti-Gr-1-AF700 (RB6-8C5, 108422), anti-B220 (CD45R)-APC-eFluor780 (RA3-6B2, 47-0452-82), anti-CD115-PE-Cy7 (AFS98, 25-1152-82), anti-CD117 (c-Kit)-BV421 (2B8, 105828), anti-F4/80-AF647 (BM8, 123122), anti-Sca-1-FITC (D7; 11-5981-85), anti-CD34-PE (MEC14.7, 119308), anti-CD135 (Flt3)-PerCP-eFluor710 (A2F10, 46-1351-80), K_i-67-PerCP-eF710 (SolA15, 46-5698-82), anti-CD45.1 BV605 (A20, 110737), anti-CD45.1-BV785 (A20, 110743), anti-CD45.2-BV650 (104, 109835), anti-Il-7R-PE (A019D5, 351303), anti-CD34-BV421 (MEC14.7, 119321), anti-CD16/32-PerCP-eF710 (93, 46-0161-82), all purchased from BioLegend or eBioscience. Unless otherwise specified, all antibodies were used at a 1:100 dilution. FACS analyses were carried out using a BD LSRII flow cytometer (BD Biosciences) and cell sorting experiments were performed using an Aria Cell Sorter (BD) or Moflow Astrios (Beckman Coulter).

Human macrophage marker analysis on human bone marrow and G-CSF mobilized HSCs

Deidentified human bone marrow and G-CSF mobilized blood samples were obtained after informed consent under institutional biospecimen procurement (#06-107) and use (#16-154) protocols reviewed and approved by the MSKCC Institutional Review Board. Cryopreserved specimens (from five females and four males, age range: 54 to 72 years) were rapidly thawed in a 37°C water bath, followed by the dropwise addition of 10 ml FACS buffer (PEB: 2 mM EDTA, 0.5% BSA, 0.05% sodium azide in PBS). Cells were centrifuged for 10 min at 300 g and resuspended at ~1 × 10^6 cells in 200 μl of fresh FACS buffer. Human Fc receptors were blocked with 5 μl per sample Human TruStain FcX (BioLegend cat#422301) for 15 min, followed by staining with human antibodies for 45 min at 4°C. Human HSCs were labeled with antibodies for CD34 (Invitrogen clone 4H11, Pe-Cy7), CD38 (Invitrogen clone HIT2, APC-eFluor780), CD90 (BioLegend clone 5E10, PE), CD45RA (BioLegend clone HI100, PerCP-Cy5.5), CD49f (BioLegend clone GoH3, BV421), and c-Kit (BioLegend clone 104D2, FITC) all at 1:50 dilution. Human macrophage markers were labeled with antibodies for CD11b (BioLegend clone M1/70, Alexa Fluor647), CD14 (BioLegend clone HCD14, APC), and CD163 (Invitrogen clone MAC 2-158, Alexa Fluor647) at dilutions of 1:50, 1:20, and 1:20 respectively. Macrophage markers were tested on THP-1 and U937 human macrophages and confirmed to label macrophage/monocyte subsets in human primary samples. Human macrophage markers were compared to an FMO control containing similar concentration of mouse IgG1k isotype antibody (BioLegend clone MOPC-21, APC) for all samples. After antibody staining, cells were washed with excess FACS buffer, centrifuged, and resuspended with FACS buffer containing DAPI for dead cell exclusion and kept on ice. Flow cytometry was performed using a BD LSRII flow cytometer and data were analyzed with FlowJo software.

RNA sequencing

Approximately 2000 to 5000 F4/80$^-$ or F4/80$^+$ HSCs were sorted into RNase- & DNase-free 1.5-ml tubes containing ~200 μl of RLT Plus buffer (RNeasy Plus Micro Kit, Qiagen). Total mRNA was extracted using the RNeasy Plus Micro kit as per instructions. mRNA integrity and quantity were assayed with an Agilent 2100 Bioanalyzer (Agilent Technologies) using a Pico RNA Chip, with all samples used in sequencing scoring ≥9.7 on RIN/RQN values. A total of three biological replicates underwent sequencing for both F4/80$^-$ or F4/80$^+$ HSC subsets. Sequencing data generated from Illumina Platform PE150 were processed using the following pipeline. In brief, reads were aligned and mapped to the mouse genome using the program HISAT2 v.2.0.5. Fragments per kilobase of transcript sequence per millions base pairs sequence (FPKM) was calculated to adjust for sequencing depth and gene length on raw counts. Differential analysis was performed using DESeq2 v.1.20.0 and edgeR v.3.22.5 using log2(FoldChange) >1 and padj set to 0.05.

RNA isolation and quantitative real-time PCR (Q-PCR)

Messenger RNA isolation was performed using Dynabeads mRNA DIRECT MicroKit (Life Technologies), and reverse transcription was performed using RNA to cDNA EcoDry Premix (Clontech) according to the manufacturer's protocols. Quantitative PCR was performed with SYBR Green (Roche) on the QuantStudio 6 Flex Real-Time PCR System (Applied Biosystems). The PCR protocol consisted of 1 cycle at 95°C (10 min) followed by 40 cycles of 95°C (15 s) and 60°C (1 min). Expression of glyceraldehyde-3-phosphate dehydrogenase (*Gapdh*) or β-actin was used as standard. The average threshold cycle number (Ct) for each tested mRNA was used to quantify the relative expression of each gene; 2 − [Ct(gene) − Ct(standard)].

DiI-incorporated liposome assay

Control liposomes were labeled with the fluorochrome DiI, and as a result the label will show their uptake by macrophages. Briefly, 10 μl DiI Solution (V-22885, Life Technologies) was added per ml liposome suspension and liposome suspension was shaken thoroughly. The mix was incubated 10 min at room temperature and centrifuged at 10,000 rpm for 10 min. The supernatant was removed, and liposomes were resuspended in sterile PBS. This washing step was performed twice, and liposomes were resuspended in Sterile PBS at the original volume. Liposomes were stored in the dark at 4°C. Prior to injection, liposomes were brought to room temperature, and 250 μl DiI-labeled liposomes were injected i.v. per mouse.

Quantification and statistical analyses

All data are represented as mean ± SEM. *n* represents the number of biological replicates or mice analyzed in each experiment, as detailed in figure legends. Comparison between two samples were done using two-tailed Student's

t tests. One-way analysis of variance (ANOVA) analyses followed by Tukey's multiple comparison test or two-way ANOVA followed by Sidak multiple comparison test were used for multiple group comparisons or multiparameter analysis. Statistical analyses were performed using GraphPad Prism 7 software. $^{*}P < 0.05$, $^{**}P < 0.01$, $^{***}P < 0.001$.

REFERENCES AND NOTES

1. S. Pinho, P. S. Frenette, Haematopoietic stem cell activity and interactions with the niche. *Nat. Rev. Mol. Cell Biol.* **20**, 303–320 (2019). doi: 10.1038/s41580-019-0103-9; pmid: 30745579
2. A. C. Wilkinson, K. J. Igarashi, H. Nakauchi, Haematopoietic stem cell self-renewal in vivo and ex vivo. *Nat. Rev. Genet.* **21**, 541–554 (2020). doi: 10.1038/s41576-020-0241-0; pmid: 32467607
3. L. M. Calvi, D. C. Link, The hematopoietic stem cell niche in homeostasis and disease. *Blood* **126**, 2443–2451 (2015). doi: 10.1182/blood-2015-07-533588; pmid: 26468230
4. S. Méndez-Ferrer, D. Lucas, M. Battista, P. S. Frenette, Haematopoietic stem cell release is regulated by circadian oscillations. *Nature* **452**, 442–447 (2008). doi: 10.1038/nature06685; pmid: 18256599
5. S. Massberg *et al*., Immunosurveillance by hematopoietic progenitor cells trafficking through blood, lymph, and peripheral tissues. *Cell* **131**, 994–1008 (2007). doi: 10.1016/j.cell.2007.09.047; pmid: 18045540
6. R. S. Welner, P. W. Kincade, Stem cells on patrol. *Cell* **131**, 842–844 (2007). doi: 10.1016/j.cell.2007.11.010; pmid: 18045530
7. J. P. Lévesque, J. Hendy, Y. Takamatsu, P. J. Simmons, L. J. Bendall, Disruption of the CXCR4/CXCL12 chemotactic interaction during hematopoietic stem cell mobilization induced by GCSF or cyclophosphamide. *J. Clin. Invest.* **111**, 187–196 (2003). doi: 10.1172/JCI15994; pmid: 12531874
8. I. Petit *et al*., G-CSF induces stem cell mobilization by decreasing bone marrow SDF-1 and up-regulating CXCR4. *Nat. Immunol.* **3**, 687–694 (2002). doi: 10.1038/ni813; pmid: 12068293
9. S. Haas, A. Trumpp, M. D. Milsom, Causes and Consequences of Hematopoietic Stem Cell Heterogeneity. *Cell Stem Cell* **22**, 627–638 (2018). doi: 10.1016/j.stem.2018.04.003; pmid: 29727678
10. M. Crisan, E. Dzierzak, The many faces of hematopoietic stem cell heterogeneity. *Development* **143**, 4571–4581 (2016). doi: 10.1242/dev.114231; pmid: 27965438
11. C. E. Muller-Sieburg, H. B. Sieburg, J. M. Bernitz, G. Cattarossi, Stem cell heterogeneity: Implications for aging and regenerative medicine. *Blood* **119**, 3900–3907 (2012). doi: 10.1182/blood-2011-12-376749; pmid: 22408258
12. K. Gustafsson, D. T. Scadden, Growing old in the age of heterogeneity: The perils of shifting clonality. *Curr. Opin. Hematol.* **26**, 222–227 (2019). doi: 10.1097/MOH.0000000000000513; pmid: 31045646
13. J. Chen *et al*., Myelodysplastic syndrome progression to acute myeloid leukemia at the stem cell level. *Nat. Med.* **25**, 103–110 (2019). doi: 10.1038/s41591-018-0267-4; pmid: 30510255
14. Y. R. Kao *et al*., An iron rheostat controls hematopoietic stem cell fate. *Cell Stem Cell* **31**, 378–397.e12 (2024). doi: 10.1016/j.stem.2024.01.011; pmid: 38402617
15. J. C. Wheat *et al*., Single-molecule imaging of transcription dynamics in somatic stem cells. *Nature* **583**, 431–436 (2020). doi: 10.1038/s41586-020-2432-4; pmid: 32581360
16. P. R. Taylor *et al*., Macrophage receptors and immune recognition. *Annu. Rev. Immunol.* **23**, 901–944 (2005). doi: 10.1146/annurev.immunol.23.021704.115816; pmid: 15771589
17. D. A. Hume, A. P. Robinson, G. G. MacPherson, S. Gordon, The mononuclear phagocyte system of the mouse defined by immunohistochemical localization of antigen F4/80. Relationship between macrophages, Langerhans cells, reticular cells, and dendritic cells in lymphoid and hematopoietic organs. *J. Exp. Med.* **158**, 1522–1536 (1983). doi: 10.1084/jem.158.5.1522; pmid: 6355361
18. C. Blériot, S. Chakarov, F. Ginhoux, Determinants of Resident Tissue Macrophage Identity and Function. *Immunity* **52**, 957–970 (2020). doi: 10.1016/j.immuni.2020.05.014; pmid: 32553181
19. U. Narayanasami *et al*., Randomized trial of filgrastim versus chemotherapy and filgrastim mobilization of hematopoietic progenitor cells for rescue in autologous transplantation. *Blood* **98**, 2059–2064 (2001). doi: 10.1182/blood.V98.7.2059; pmid: 11567990
20. H. E. Broxmeyer *et al*., Rapid mobilization of murine and human hematopoietic stem and progenitor cells with AMD3100, a CXCR4 antagonist. *J. Exp. Med.* **201**, 1307–1318 (2005). doi: 10.1084/jem.20041385; pmid: 15837815
21. S. Hatse, K. Princen, G. Bridger, E. De Clercq, D. Schols, Chemokine receptor inhibition by AMD3100 is strictly confined to CXCR4. *FEBS Lett.* **527**, 255–262 (2002). doi: 10.1016/S0014-5793(02)03143-5; pmid: 12220670
22. A. Chow *et al*., Bone marrow CD169+ macrophages promote the retention of hematopoietic stem and progenitor cells in the mesenchymal stem cell niche. *J. Exp. Med.* **208**, 261–271 (2011). doi: 10.1084/jem.20101688; pmid: 21282381
23. M. J. Christopher, M. Rao, F. Liu, J. R. Woloszynek, D. C. Link, Expression of the G-CSF receptor in monocytic cells is sufficient to mediate hematopoietic progenitor mobilization by G-CSF in mice. *J. Exp. Med.* **208**, 251–260 (2011). doi: 10.1084/jem.20101700; pmid: 21282380
24. I. G. Winkler *et al*., Bone marrow macrophages maintain hematopoietic stem cell (HSC) niches and their depletion mobilizes HSCs. *Blood* **116**, 4815–4828 (2010). doi: 10.1182/blood-2009-11-253534; pmid: 20713966
25. Z. Xing *et al*., Increased hematopoietic stem cell mobilization in aged mice. *Blood* **108**, 2190–2197 (2006). doi: 10.1182/blood-2005-12-010272; pmid: 16741255
26. W. W. Pang, S. L. Schrier, I. L. Weissman, Age-associated changes in human hematopoietic stem cells. *Semin. Hematol.* **54**, 39–42 (2017). doi: 10.1053/j.seminhematol.2016.10.004; pmid: 28088986
27. K. Karasawa *et al*., Vascular-resident CD169-positive monocytes and macrophages control neutrophil accumulation in the kidney with ischemia-reperfusion injury. *J. Am. Soc. Nephrol.* **26**, 896–906 (2015). doi: 10.1681/ASN.2014020195; pmid: 25266072
28. P. R. Crocker, S. Gordon, Properties and distribution of a lectin-like hemagglutinin differentially expressed by murine stromal tissue macrophages. *J. Exp. Med.* **164**, 1862–1875 (1986). doi: 10.1084/jem.164.6.1862; pmid: 3783087
29. A. Mantovani *et al*., The chemokine system in diverse forms of macrophage activation and polarization. *Trends Immunol.* **25**, 677–686 (2004). doi: 10.1016/j.it.2004.09.015; pmid: 15530839
30. T. Sugiyama, H. Kohara, M. Noda, T. Nagasawa, Maintenance of the hematopoietic stem cell pool by CXCL12-CXCR4 chemokine signaling in bone marrow stromal cell niches. *Immunity* **25**, 977–988 (2006). doi: 10.1016/j.immuni.2006.10.016; pmid: 17174120
31. J. M. Busillo, J. L. Benovic, Regulation of CXCR4 signaling. *Biochim. Biophys. Acta* **1768**, 952–963 (2007). doi: 10.1016/j.bbamem.2006.11.002; pmid: 17169327
32. Y. Kunisaki *et al*., Arteriolar niches maintain haematopoietic stem cell quiescence. *Nature* **502**, 637–643 (2013). doi: 10.1038/nature12612; pmid: 24107994
33. Y. Miyake *et al*., Critical role of macrophages in the marginal zone in the suppression of immune responses to apoptotic cell-associated antigens. *J. Clin. Invest.* **117**, 2268–2278 (2007). doi: 10.1172/JCI31990; pmid: 17657313
34. H. D. Danenberg *et al*., Macrophage depletion by clodronate-containing liposomes reduces neointimal formation after balloon injury in rats and rabbits. *Circulation* **106**, 599–605 (2002). doi: 10.1161/01.CIR.0000023532.98469.48; pmid: 12147543
35. S. Kaur *et al*., Self-repopulating recipient bone marrow resident macrophages promote long-term hematopoietic stem cell engraftment. *Blood* **132**, 735–749 (2018). doi: 10.1182/blood-2018-01-829663; pmid: 29945953
36. M. D. Muzumdar, B. Tasic, K. Miyamichi, L. Li, L. Luo, A global double-fluorescent Cre reporter mouse. *Genesis* **45**, 593–605 (2007). doi: 10.1002/dvg.20335; pmid: 17868096
37. B. C. Schaefer, M. L. Schaefer, J. W. Kappler, P. Marrack, R. M. Kedl, Observation of antigen-dependent CD8+ T-cell/dendritic cell interactions in vivo. *Cell. Immunol.* **214**, 110–122 (2001). doi: 10.1006/cimm.2001.1895; pmid: 12088410
38. E. Joly, D. Hudrisier, What is trogocytosis and what is its purpose? *Nat. Immunol.* **4**, 815 (2003). doi: 10.1038/ni0903-815; pmid: 12942076
39. D. M. Davis, Intercellular transfer of cell-surface proteins is common and can affect many stages of an immune response. *Nat. Rev. Immunol.* **7**, 238–243 (2007). doi: 10.1038/nri2020; pmid: 17290299
40. K. Miyake *et al*., Trogocytosis of peptide-MHC class II complexes from dendritic cells confers antigen-presenting ability on basophils. *Proc. Natl. Acad. Sci. U.S.A.* **114**, 1111–1116 (2017). doi: 10.1073/pnas.1615973114; pmid: 28096423
41. V. C. Broudy, Stem cell factor and hematopoiesis. *Blood* **90**, 1345–1364 (1997). doi: 10.1182/blood.V90.4.1345; pmid: 9269751
42. M. C. Heinrich *et al*., Inhibition of c-kit receptor tyrosine kinase activity by STI 571, a selective tyrosine kinase inhibitor. *Blood* **96**, 925–932 (2000). doi: 10.1182/blood.V96.3.925; pmid: 10910906
43. J. Lennartsson, L. Rönnstrand, Stem cell factor receptor/c-Kit: From basic science to clinical implications. *Physiol. Rev.* **92**, 1619–1649 (2012). doi: 10.1152/physrev.00046.2011; pmid: 23073628
44. K. Masson, E. Heiss, H. Band, L. Rönnstrand, Direct binding of Cbl to Tyr568 and Tyr936 of the stem cell factor receptor/c-Kit is required for ligand-induced ubiquitination, internalization and degradation. *Biochem. J.* **399**, 59–67 (2006). doi: 10.1042/BJ20060464; pmid: 16780420
45. S. Zeng, Z. Xu, S. Lipkowitz, J. B. Longley, Regulation of stem cell factor receptor signaling by Cbl family proteins (Cbl-b/c-Cbl). *Blood* **105**, 226–232 (2005). doi: 10.1182/blood-2004-05-1768; pmid: 15315962
46. R. Henschler, A. Piiper, R. Bistrian, D. Möbest, SDF-1alpha-induced intracellular calcium transient involves Rho GTPase signalling and is required for migration of hematopoietic progenitor cells. *Biochem. Biophys. Res. Commun.* **311**, 1067–1071 (2003). doi: 10.1016/j.bbrc.2003.10.112; pmid: 14623290
47. J. Hamann *et al*., EMR1, the human homolog of F4/80, is an eosinophil-specific receptor. *Eur. J. Immunol.* **37**, 2797–2802 (2007). doi: 10.1002/eji.200737553; pmid: 17823986
48. J. Y. Shin, W. Hu, M. Naramura, C. Y. Park, High c-Kit expression identifies hematopoietic stem cells with impaired self-renewal and megakaryocytic bias. *J. Exp. Med.* **211**, 217–231 (2014). doi: 10.1084/jem.20131128; pmid: 24446491
49. L. B. To *et al*., A comparative study of the phenotype and proliferative capacity of peripheral blood (PB) CD34+ cells mobilized by four different protocols and those of steady-phase PB and bone marrow CD34+ cells. *Blood* **84**, 2930–2939 (1994). doi: 10.1182/blood.V84.9.2930.2930; pmid: 7524760
50. R. G. Andrews *et al*., In vivo synergy between recombinant human stem cell factor and recombinant human granulocyte colony-stimulating factor in baboons enhanced circulation of progenitor cells. *Blood* **84**, 800–810 (1994). doi: 10.1182/blood.V84.3.800.800; pmid: 7519077
51. A. Chow *et al*., CD169^{+} macrophages provide a niche promoting erythropoiesis under homeostasis and stress. *Nat. Med.* **19**, 429–436 (2013). doi: 10.1038/nm.3057; pmid: 23502962
52. P. Ramos *et al*., Macrophages support pathological erythropoiesis in polycythemia vera and β-thalassemia. *Nat. Med.* **19**, 437–445 (2013). doi: 10.1038/nm.3126; pmid: 23502961
53. M. Albiero *et al*., Bone Marrow Macrophages Contribute to Diabetic Stem Cell Mobilopathy by Producing Oncostatin M. *Diabetes* **64**, 2957–2968 (2015). doi: 10.2337/db14-1473; pmid: 25804939
54. S. Nakandakari-Higa *et al*., Universal recording of immune cell interactions in vivo. *Nature* **627**, 399–406 (2024). doi: 10.1038/s41586-024-07134-4; pmid: 38448581
55. R. K. Hopman, J. F. DiPersio, Advances in stem cell mobilization. *Blood Rev.* **28**, 31–40 (2014). doi: 10.1016/j.blre.2014.01.001; pmid: 24476957

ACKNOWLEDGMENTS

We are deeply saddened by the loss of Paul Frenette on 26 July 2021. His scientific excellence, creativity, and rigor laid the foundation for this manuscript and will continue to inspire us and many of his mentees and colleagues to pursue better science. He has been fondly remembered and greatly missed by all, and his legacy will live on through his discoveries and trainees. We thank M. Tanaka for providing the CD169-Cre and CD169-DTR mice. We are grateful to C. Prophete for technical assistance and D. Sun from the Human Stem Cell FACS and Xenotransplantation Facility for assistance with cell sorting, S. Sharma and M. Rangesa from Memorial Sloan Kettering Cancer Center for assistance with human sample acquisition. and T. A. Harris from the Einstein Creative Services team for illustrating the working model scheme.

Funding: This work was supported by grants from the NIH [U01DK116312, R01DK056638, R01DK112976, and R01HL069438 (to P.S.F.); DK10513 and CA230756 (to B.W.); R01HL157948 (to U.S. and B.W.); and R35CA253127 (to U.S.)]. X.G. was supported by the American Society of Hematology (ASH) Fellow-to-Faculty Scholar Award and the NIH K01 award (DK137045). M.M. is supported by the ASH Junior Faculty Scholar Award (2023) and previously by the European Molecular Biology Organization (EMBO) European Commission FP7 (Marie Curie Actions; EMBOCOFUND2012, GA-2012-600394, and ALTF 447-2014), a New York Stem Cell Foundation (NYSCF) Druckenmiller Fellowship (2017), and an ASH Research Restart Award (2020). P.E.B was supported by a postdoctoral fellowship from Fonds de recherche du Québec-Santé (FRQS, 2015-2018). R.S.C. was supported by a National Heart, Lung, and Blood Institute (NHLBI) T32 training grant (T32 HL144456) and an NHLBI F32 Ruth L. Kirschstein Individual National Research Service Award (F32 HL158084), as well as a Gottesman Stem Cell Institute Paul S. Frenette Scholar Award. R.S.C. is currently supported by a Cancer Research Institute Irvington Postdoctoral Fellowship (CRI4994). H.L. is the recipient of a NIH K01 Research Scientist Development Award (DK131401). U.S. holds the Edward P. Evans Endowed Professorship in Myelodysplastic Syndromes at Albert Einstein College of Medicine supported by the Edward P. Evans Foundation. B.W. is the Diane and Arthur B. Belfer Scholar in Cancer Research at Albert Einstein College of Medicine and a Leukemia and Lymphoma Society Scholar.
Author contributions: P.S.F. designed and supervised the study, interpreted data, and wrote the initial manuscript. X.G., R.S.C., and P.E.B. designed the study, performed the experiments, analyzed data, and wrote the manuscript; M.M., D.Z., C.R.M., H.L., and M.S. helped with experiments. D.J.C. provided the human bone marrow and mobilized peripheral blood samples and provided valuable inputs on the manuscript. U.S. and B.W. interpreted data, designed the study, supervised multiple submissions and revisions, and wrote the final manuscript. All authors discussed the results and commented on the manuscript. **Competing interests:** P.S.F. served as a consultant for Pfizer, received research funding from Ironwood Pharmaceuticals, and was a shareholder of Cygnal Therapeutics. U.S. has received research funding from GlaxoSmithKline, Bayer HealthCare, and Aileron Therapeutics; has received compensation for consultancy services and for serving on scientific advisory boards from GlaxoSmithKline, Bayer HealthCare, Celgene, Aileron Therapeutics, Stelexis Therapeutics, Pieris Pharmaceuticals, Trillium Therapeutics, and Novartis; and has equity ownership in and is serving on the board of directors of Stelexis Therapeutics. B.W. has received funds for research projects from Novartis Pharmaceuticals, Aileron Therapeutics, and Life Biosciences, as well as from serving on advisory boards of Novartis Pharmaceuticals. The other authors declare that they have no competing interests. **Data and materials availability:** All data needed to evaluate the conclusions in the paper are present in the paper or the supplementary materials. RNA sequencing data are accessible at Gene Expression Omnibus (GSE267632). Model animals are available from corresponding authors upon request; C57BL/6-Siglec1(cre)^{Mtaka}-CD169-cre mice were obtained and used in accordance with a material transfer agreement (RIKEN).

SUPPLEMENTARY MATERIALS

science.org/doi/10.1126/science.adp2065
Figs. S1 to S5
MDAR Reproducibility Checklist

Submitted 12 March 2024; accepted 14 June 2024
10.1126/science.adp2065